Rev.Adv.Mater.Sci. 18(2008) 448-453

STABILITY OF AMORPHOUS Al ALLOYS DURING INTENSE DEFORMATION AND ANNEALING

J.H. Perepezko[1], J. Hamann[2], R.J. Hebert[1] and H. Rösner[3]

[1]Department of Materials Science and Engineering, University of Wisconsin-Madison, 1509 University Avenue, Madison, WI 53706, USA
[2] Xtalic Corporation, 200 Boston Ave., Suite 4100, Medford, MA, 02155, USA
[3]Forschungszentrum Karlsruhe, P.O. Box 3640, 76021 Karlsruhe, Germany

Received: March 29, 2008

Abstract. Microstructures based upon a dispersion of primary nanocrystals in an amorphous matrix greatly affect mechanical and corrosion properties. The addition of only 1 at.% of Cu to an amorphous Al-Sm-Ni alloy is an effective microstructure control by narrowing the size distribution of Al nanocrystals and reduces the average size of the nanocrystals from 10 nm to about 7.5 nm while increasing the particle number density. Calorimetry analyses of primary crystallization reaction suggest that the addition of Cu modifies the atomic arrangement and induces structural heterogeneities that could act as nucleation sites with a distribution of potencies. Atom probe field ion microscopy and TEM studies have revealed in addition that Cu atoms remain unclustered in the amorphous matrix. As another method of microstructure control dispersions of Al nanocrystals can be obtained during intense deformation at room-temperature. With increasing strain, the initial concentration of nanocrystals in shear bands develops into a homogeneous distribution throughout the sample. Moreover, at true strain levels of about –11, only Al has crystallized in the amorphous matrix, while primary crystallization of Al can not be obtained during annealing of the same amorphous $Al_{85}Y_{10}Fe_5$ alloy. The strong composition dependence of the crystallization reactions and resulting microstructures reflects not only underlying thermodynamic constraints, but also indicates a strong composition dependence of the amorphous atomic arrangement.

1. INTRODUCTION

One of the highlights in the development of unique microstructures synthesized by rapid solidification or by intense deformation is the common occurrence of various metastable structural states that often develop with nanostructured size scales. Whether these evolving microstructures represent ultrafine grain sizes, supersaturated compositions of equilibrium phases, or non-equilibrium phase structures, their development has significantly expanded the range of microstructural options that are available for the synthesis of new materials and the attainment of new levels of performance. Amorphous alloys, for example, represent a class of materials that reveals exceptional properties such as high strength and resilience [1,2], and often outstanding corrosion properties resulting from the metastable, non-periodic atomic arrangement [3]. Dispersions of nanocrystals in the amorphous matrix have been found to improve the mechanical strength levels further [1,4]. Therefore, much attention has been devoted to understanding the devitrification reactions in order to control the nanocrystal size distribution and particle number densities [5,6].

The experience on devitrification behavior indicates that for some amorphous alloys changes in composition as small as 2 at.% can change the

Corresponding author: J.H. Perepezko, e-mail: perepezk@engr.wisc.edu

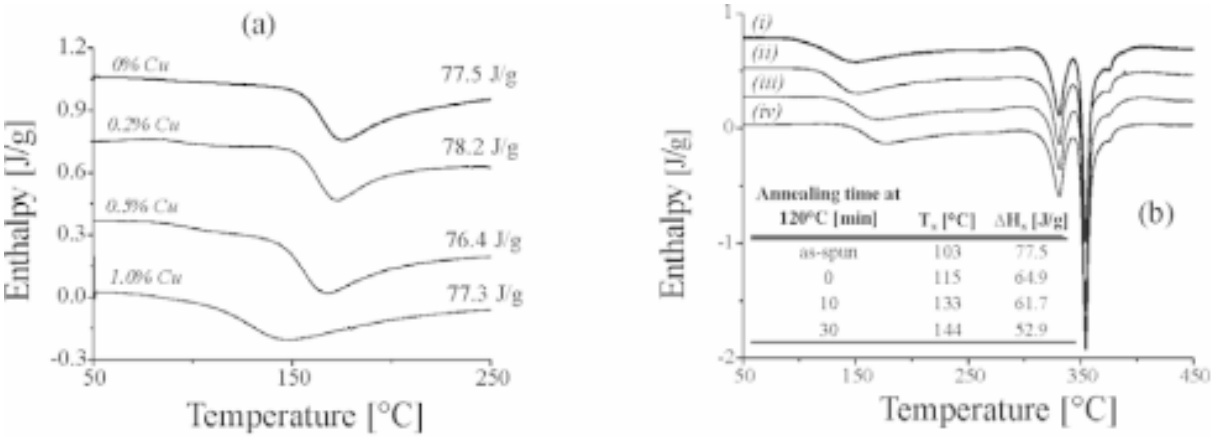

Fig. 1. (a) DSC traces (*dT*/*dt* = 20 °C/min) of $Al_{88}Ni_{8-x}Sm_4Cu_x$ MSR samples ; as the crystallization onset shifts to lower temperatures with greater Cu addition, the integrated crystallization enthalpy remains constant. (b) Continuous heating DSC traces of $Al_{88}Ni_7Sm_4Cu_1$ following thermal cycling treatment around 120 °C. Also included is a summary of the integrated crystallization enthalpies and subtracted DSC traces to illustrate, how the annealing treatments affect the primary crystallization behavior. (i) as-spun, (ii) cycled around 120 °C, (iii) 10 min anneal at 120 °C, (iv) 30 min anneal at 120 °C.

crystallization behavior significantly. For example, the glass transition signal in amorphous Al-Ni-Ce, Al-Y-Fe, or Al-Sm alloys, for example, is often concealed by the onset of primary crystallization [6-8]. Still, it is possible to change the solute level in select Al-based glasses by as little as 2 at.% to produce an amorphous alloy that displays an endothermic signal prior to crystallization during heating, thereby altering the nanocrystallization response [6]. This change in nanocrystallization response with small compositional changes is not limited to Al-based glasses, but has also been observed in Fe- and Zr-based glasses [9,10]. However, it is not a general feature of all metallic glasses. Numerous studies indicate furthermore that partial substitution of small amounts of Cu or Ag for the transition metal component in some Al-TM-RE (TM = transition metal; RE = rare earth metal) systems effectively refines the size and increases the density of primary phase nanocrystals precipitated from the amorphous precursor material [11-13]. In an amorphous Fe-based alloy containing 1 at.% Cu, atom probe field ion microscopy (APFIM) has confirmed the notion of clustering of the Cu additions [14]. In contrast to Fe-base glasses where Cu clusters act as heterogeneous nucleation sites, the addition of 1 at.% Cu to an amorphous Al-Ni-Sm alloy refines the average primary Al nc size, but does not result in the formation of clusters of Cu atoms following an annealing treatment in the primary crystallization regime [13]. This result is in agreement with previous work, demonstrating that the substitution of 1 at.% Cu for Ni in several Al-Ni-Ce and Al-Ni-Y compositions reduces the average size of primary Al nanocrystals [11,12]. Further advances in understanding the saturation limit for dopant induced microstructure refinement (i.e. Cu for Ni in $Al_{88}Ni_8Sm_4$) can be accomplished by coupling results from continuous heating DSC analysis with a size distribution analysis identifying the nanocrystal density and average diameter as a function of Cu content in annealed melt-spun ribbon samples.

A strong composition dependence of the crystallization reactions has moreover been observed for deformation-induced crystallization reactions in amorphous Al-Ni-Ce alloys. During bending, nanocrystals developed within shear-bands of an amorphous $Al_{87}Ni_{10}Ce_3$ alloy, but did not develop under the same deformation conditions for an amorphous $Al_{85}Ni_{10}Ce_5$ alloy [15]. There is also a dependence on stress state [16]. Further the strong composition dependence has also been observed for cold-rolling as well [17,18].

The strong composition dependence of crystallization reactions in amorphous Al alloys is high-

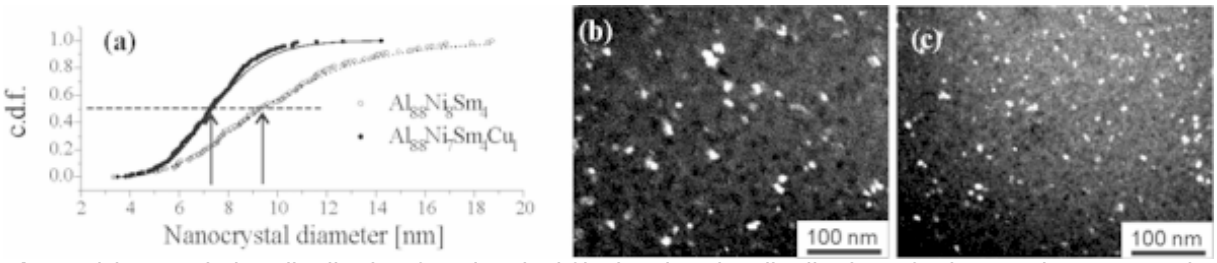

Fig. 2. (a) Cumulative distribution function (c.d.f.) showing the distribution of primary Al nanocrystals; DFTEM micrographs of primary Al nanocrystals in (b) $Al_{88}Ni_8Sm_4$ and (c) $Al_{88}Ni_7Sm_4Cu_1$.

lighted in the following with an example of Cu-addition to an amorphous $Al_{88}Ni_8Sm_4$ alloy and results obtained from intense deformation of amorphous Al-Y-Fe alloys. The analysis of deformed amorphous samples shows in addition that with increasing strain a homogeneous dispersion of nanocrystals develops throughout the sample. The results indicate novel approaches to control the atomic arrangement in amorphous alloys and the development of nanocrystals.

2. PRIMARY CRYSTALLIZATION OF Cu-DOPED Al88Ni8Sm4

Selective substitutions of Cu for Ni in $Al_{88}Ni_{8-x}Sm_4Cu_x$ melt-spun ribbon samples (x = at.% Cu, ranging from 0.2 $\rightarrow$ 1 at.%, melt-spinning at a wheel speed of 55 m/s) shift the calorimetrically measured onset of primary crystallization to successively lower temperatures with increasing amount of Cu substitution (Fig. 1). The integrated enthalpy of the primary crystallization exotherm (normalized by sample mass) does not change appreciably with Cu substitution level indicating that the volume of amorphous precursor material transforming to primary Al nanocrystals remains essentially constant. Further, the shape of the primary exothermic onset changes from a sharp deviation from a horizontal baseline to a more shallow depression extending over a wider temperature range. Microstructure analysis of ribbon samples of $Al_{88}Ni_8Sm_4$ and $Al_{88}Ni_7Sm_4Cu_1$ annealed for 30 minutes at the onset of primary crystallization for each composition (estimated with DSC to be 154 and 104 °C respectively) indicate that the average size of the primary phase nanocrystals is reduced by nearly 25% from about 10 nm to about 7.5 nm with Cu substitution (Fig. 2). The estimated nanocrystal density increased from $9 \cdot 10^{21}$ to $1.6 \cdot 10^{22}$ m^{-3} with substitution of 1 at.% Cu for Ni in the base alloy composition. These estimates were based on analysis of a composite micrograph obtained by overlaying four separate DFTEM micrographs taken with the objective aperture placed at four symmetric clock positions around the primary diffraction ring and with sample thickness measurements obtained from electron energy loss spectroscopy (EELS) on a LEO912 energy filtered TEM (EFTEM).

Atom probe results have shown that in Al-based glasses containing small amounts of Cu, the Cu atoms are distributed homogeneously in the amorphous matrix [12,13]. Since TEM and atom probe analyses have not yet provided a conclusive explanation of how the small Cu substitutions refine the grain size in amorphous Al-based alloys, further calorimetry investigations were performed to explore whether the broad shape of the primary crystallization exotherm present in the $Al_{88}Ni_7Sm_4Cu_1$ could be due to crystallization events driven by multiple heterogeneities (i.e. Al clusters retained during the quench and/or Cu atoms or clusters). The gradual broadening of the primary crystallization onset with increased Cu substitution level suggests that independent primary crystallization events are taking place over a broad temperature range, with the earliest nucleation events being catalyzed by a more potent heterogeneity than is present in the alloy containing no Cu. To explore this hypothesis, replicate as-solidified $Al_{88}Ni_7Sm_4Cu_1$ ribbon samples were heated to 120 °C and annealed for 0, 10, and 30 minutes respectively. Following the annealing treatment, the

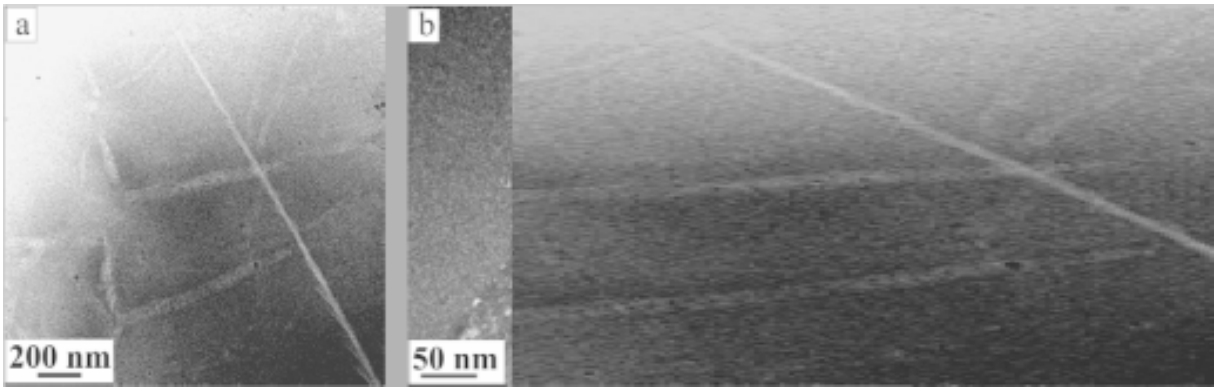

Fig. 3. (a) Bright-field TEM image of a cold-rolled amorphous $Al_{88}Y_7Fe_5$ alloy at a true strain of –0.74. Bright bands in the image depict shear bands. (b) Dark-field TEM image of the same alloy showing nanocrystals inside shear bands. (c) Amorphous $Al_{88}Y_7Fe_5$ alloy at a true strain of approximately –11.

samples were immediately quenched to room temperature, and then re-heated through crystallization. By comparing the change in primary crystallization enthalpy between the as-solidified sample and each annealed sample, the fraction of material transformed from the amorphous precursor phase to primary Al nanocrystals was estimated. Balancing the enthalpy of primary crystallization of the as-spun alloy with the total enthalpy of crystallization (primary and intermetallic), it is determined that approximately 44% of the material is available for transformation to α-Al. Data in Fig. 3 indicates that there is an initial burst of nucleation during a cycle around 120 °C (isothermal holding time = 0 min.) whereby 7.1% of the material has transformed to Al nanocrystals. Following 10 and 30-minute isothermal holding treatments at 120 °C, an additional 1.8 and 6.8% (respectively) of the microstructure transforms to primary Al nanocrystals. These results indicate that upon heating the as-solidified material from room temperature to the isothermal annealing temperature (120 °C) at 20 °C/min, nearly the same volume of material transforms from the amorphous precursor phase to primary Al nanocrystals as transforms during the 30 minute annealing treatment at 120 °C. Complementing the TEM size distribution results, it is evident that nucleation of a high density of primary phase nanocrystals is catalyzed at low temperatures (when diffusion is slow) by a heterogeneity not present in the base composition without Cu. The broadening of the primary crystallization exotherm and the reduction of mean nanocrystal size (with a narrowed size distribution) with the substitution of 1 at.% Cu for Ni in this alloy system are original characteristics that imply that the presence of Cu restricts growth of the primary phase. Growth restriction as a result of RE atom pile-up at the interface can explain why there is little growth of α-Al nanocrystals following the initial burst of nucleation during heating, however further studies must be completed to clarify how small amounts of Cu can substantially restrict nanocrystal. growth.

4. SHEAR BAND EVOLUTION AND CRYSTALLIZATION IN DEFORMED AMORPHOUS ALLOYS

Amorphous alloys respond to intense deformation with an inhomogeneous flow and the formation of shear bands, if the deformation takes place at temperatures well below the glass transition temperature and at high stress levels [10]. Shear bands reveal a width of about 10-80 nm in TEM images. Although a systematic investigation of the volume fraction of shear bands has not been conducted, TEM images such as the image depicted in Fig. 4a suggest that the volume fraction at early deformation stages (true strain of about –0.7 as depicted in Fig. 4a) amounts to only a few percent. Nanocrystals develop during initial deformation mostly in shear bands as the dark-field TEM image in Fig. 4b highlights. The TEM analysis of the deformed amorphous $Al_{88}Y_7Fe_5$ alloy shows that

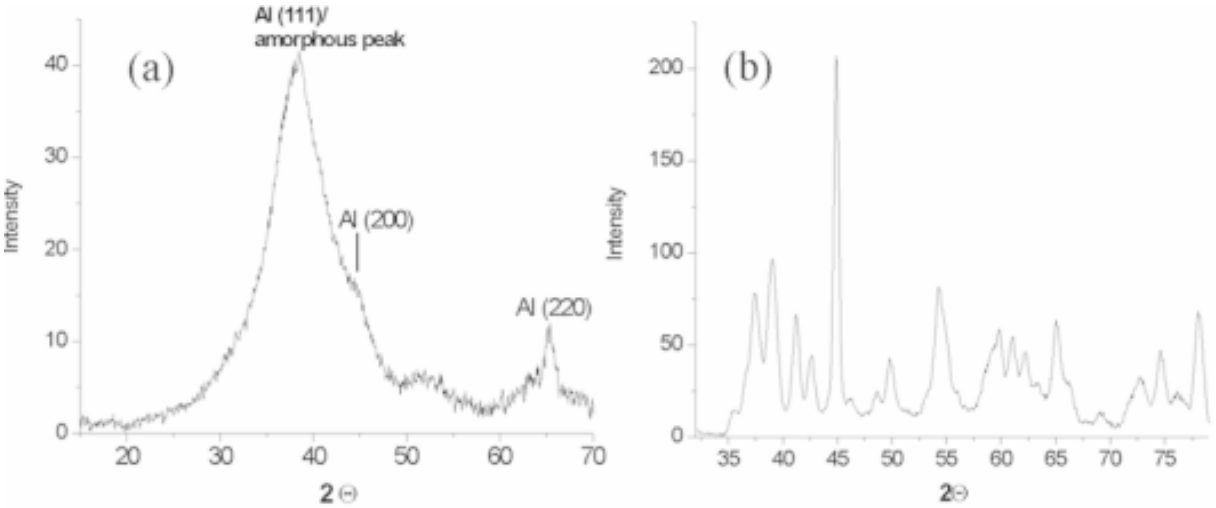

Fig. 4. (a) X-ray pattern of amorphous $Al_{85}Y_{10}Fe_5$ alloy at a true strain of about –11. (b) Amorphous $Al_{85}Y_{10}Fe_5$ alloy after annealing at 300 °C for 15 min.

at a true strain of approximately –11, a microstructure develops with nanocrystals distributed homogeneously in the amorphous matrix on the scale of the TEM imaging, i.e., at least over a distance of approximately 1 mm, as seen in Fig. 4c. Moreover, shear bands cannot easily be observed in the TEM image in Fig. 4c, although the arrangement of nanocrystals along the white dashed lines that were added to the image could reflect the presence of shear bands. The comparison between the TEM images at low strain (ε_{true} = -0.74) in Fig. 4b and at the higher strain in Fig. 4c suggests a transition from a sample with shear bands and the deformation confined only to shear bands to a deformation mode that appears to affect the entire sample, possibly by overlap of multiple shear bands or by affecting the matrix surrounding the shear bands as well. Further work is necessary, however, to identify in more detail the evolution of the shear band volume fraction with increasing strain. It should be noted that the transition from a microstructure with nanocrystals in shear bands to a microstructure of nanocrystals distributed homogeneously throughout the matrix is also observed for high-pressure torsion pressing of the amorphous $Al_{88}Y_7Fe_5$ alloy [16] and therefore appears to be an effect that is not limited to the specific deformation mode.

At true strain levels of about –5, deformation-induced crystallization occurs only for amorphous Al alloys that reveal primary crystallization during thermal processing such as the $Al_{88}Y_7Fe_5$ alloy. At higher strain levels, however, primary crystallization of Al occurs moreover for the $Al_{85}Y_{10}Fe_5$ alloy that does not reveal primary crystallization of Al during annealing as shown in Fig. 5a. The X-ray pattern clearly reveals Al-peaks superposed on the amorphous peak without additional crystalline peaks. By contrast, an X-ray pattern is shown in Fig. 5b of the undeformed sample annealed at the onset of the first exothermic signal in a continuous heating DSC experiment at 318 °C for 20 min. The X-ray pattern shows that more than one phase has developed. This result can be rationalized, if the composition dependence of the driving force is taken into account. At higher solute levels as revealed by the $Al_{85}Y_{10}Fe_5$ alloy compared with, for example, the $Al_{88}Y_7Fe_5$ alloy, the driving force for primary crystallization is reduced to a level that could be insufficient to induce crystallization for existing precursors such as quench-retained structural heterogeneities. The athermal atomic re-arrangement during the intense deformation process, on the other hand, appears to promote the formation of fcc-phases from quench-retained structural heterogeneities even at diminished driving forces.

5. SUMMARY

The systematic DSC analysis of amorphous $Al_{88}Ni_7Sm_4Cu_1$ alloys along with a TEM analysis of

partially devitrified samples has demonstrated the important effect of the Cu addition on the size and the number density of the Al nanocrystals. Rather than clustering into heterogeneous nucleation sites, the results indicate that the Cu addition modifies the atomic arrangement of the matrix. The continuous lowering of the primary crystallization onset with increasing Cu content reflects a new level of microstructure control without changing the primary crystallization behavior. In the same vein, homogeneous nanocrystal dispersions can now be obtained from intense deformation experiments at room temperature. The deformation experiments have even shown that primary phases can develop for alloy compositions that reveal complex crystallization reactions during annealing. These results offer novel opportunities to synthesize nanostructured microstructures and highlight the role of local atomic arrangements and their effect on crystallization.

ACKNOWLEDGEMENTS

Support for this work was received initially from the ARO (DAAD 19-01-1-0486). JHP is grateful for a Sabbatical Fellowship from the Forschungszentrum Karlsruhe, Germany.

REFERENCES

[1] A. Inoue // *Progr. Mat. Sci.* **43** (1998) 365.
[2] M.A. Ashby and A.L. Greer // *Scripta Mater.* **54** (2006) 321.
[3] M. Naka, K. Hashimoto and T. Masumoto // *J. Non-Cryst. Solids* **29** (1978) 61.
[4] H. Chen, Y. He, G.J. Shiflet and S.J. Poon // *Scripta Met. Mat.* **25** (1991) 1421.
[5] J.H. Perepezko, R.J. Hebert and G. Wilde // *Mater. Sci. Engr. A* **375/377** (2002) 171.
[6] D. V. Louzguine-Luzgin and A. Inoue // *Jnl. Alloys Compounds* **399** (2005) 78.
[7] D.R. Allen, J.C. Foley and J.H. Perepezko // *Acta Mater.* **46** (1998) 431.
[8] R.F. Cochrane, P. Schumacher and A.L. Greer // *Mater. Sci. Engr. A* **133** (1991) 367.
[9] M. Nakamura, Y. Hirotsu, K. Anazawa, A. Makino, A. Inoue and T. Masumoto // *Mater. Sci. Engr. A* **179/180** (1994) 487.
[10] X. Tang, J. Loeffler and W.L. Johnson // *Advances in Metallic Glasses* **317** (2002) 118.
[11] A. Inoue, K. Nakazato, Y. Kawamure and T. Masumoto // *Mat. Sci. Engr. A* **179/180** (1994) 654.
[12] S.J. Hong, P.J. Warren and B.S. Chun // *Mat. Sci. Engr. A* **304/306** (2001) 362.
[13] Y. Zhang, P.J. Warren and A. Cerezo // *Mat. Sci. Engr. A* **327** (2002) 109.
[14] K. Hono, D.H. Ping, M. Ohnuma and H. Onodera // *Acta Mater.* **47** (1999) 997.
[15] H. Chen, Y.He, G.J. Shiflet and S.J. Poon // *Nature* **367** (1994) 541.
[16] N. Boucharat, R.J. Hebert, G. Wilde and R. Z. Valiev // *Scripta Mater.* **53** (2005) 823.
[17] R.J. Hebert and J.H. Perepezko // *Mater. Sci. Engr. A* **375/377** (2004) 728.
[18] W.H. Jiang and M. Atzmon // *Acta Mater.* **51** (2003) 4095.